An absolute calibration method of an ethyl alcohol biosensor based on wavelength-modulated differential photothermal radiometry

Yi Jun Liu, Andreas Mandelis' , and Xinxin Guo

Citation: Review of Scientific Instruments **86**, 115003 (2015); doi: 10.1063/1.4935308
View online: http://dx.doi.org/10.1063/1.4935308
View Table of Contents: http://aip.scitation.org/toc/rsi/86/11
Published by the American Institute of Physics

An absolute calibration method of an ethyl alcohol biosensor based on wavelength-modulated differential photothermal radiometry

Yi Jun Liu,[1,2] Andreas Mandelis,[1,2,a)] and Xinxin Guo[1]
[1]*Department of Mechanical and Industrial Engineering, Center for Advanced Diffusion-Wave Technologies (CADIFT), University of Toronto, Toronto, Ontario M5S 3G8, Canada*
[2]*Institute of Biomaterials and Biomedical Engineering, University of Toronto, Toronto, Ontario M5S 3G9, Canada*

(Received 26 August 2015; accepted 26 October 2015; published online 20 November 2015)

In this work, laser-based wavelength-modulated differential photothermal radiometry (WM-DPTR) is applied to develop a non-invasive in-vehicle alcohol biosensor. WM-DPTR features unprecedented ethanol-specificity and sensitivity by suppressing baseline variations through a differential measurement near the peak and baseline of the mid-infrared ethanol absorption spectrum. Biosensor signal calibration curves are obtained from WM-DPTR theory and from measurements in human blood serum and ethanol solutions diffused from skin. The results demonstrate that the WM-DPTR-based calibrated alcohol biosensor can achieve high precision and accuracy for the ethanol concentration range of 0-100 mg/dl. The high-performance alcohol biosensor can be incorporated into ignition interlocks that could be fitted as a universal accessory in vehicles in an effort to reduce incidents of drinking and driving. © *2015 AIP Publishing LLC.* [http://dx.doi.org/10.1063/1.4935308]

I. INTRODUCTION

In Canada, alcohol-impaired driving is the leading cause of criminal deaths.[1] Police in 2011 reported 90 277 impaired driving incidents in which the drivers' blood alcohol concentration (BAC) was over the legal limit of 0.08 g/dl, which is about 3000 more incidents than in 2010.[1,2] While current countermeasures such as fines, incarceration, license revocations and vehicle impoundments are ineffective in preventing drunk driving because they do not modify violators' driving habits, studies have indicated that ignition interlock devices (IIDs) which may be installed in the vehicles of those convicted of driving while intoxicated (DWI) can reduce recidivism by about two thirds. However, the probability of arrest while driving with BAC over the legal limit is about one in 200.[3,4] Mothers Against Drunk Driving (MADD) has called for ignition interlocks for all convicted drunk drivers.[5] Current IIDs are sensitive to changes in the environment, use significant energy for heating, take a long time to perform a measurement, exhibit some drift in response, and require very frequent maintenance and calibration services. In addition, they require the driver to deliver a delicate breath into the device before starting the vehicle and run random retests during driving, thereby distracting the driver from the driving task.[6]

An effort is underway to develop alcohol detection technologies that could be fitted in vehicles and should be non-invasive, reliable, durable, quick to use, seamless with the driving task and require little or no maintenance.[7] Alcohol detection technologies can be grouped into one of four technology types: (1) tissue spectrometry that estimates BAC from a near-infrared (NIR) beam diffusely reflected from the interstitial fluid (ISF) in the dermis of the subject's skin;[8] (2) distant spectrometry that analyzes BAC by using measurements of exhaled carbon dioxide (CO_2) based on mid-infrared (MIR) spectroscopy as an indication of the degree of dilution of the alcohol in exhaled air; (3) fuel-cell based electrochemical devices in which BAC is determined from the current produced by the oxidation of ethanol; and (4) a behavioral system that attempts to identify cues of typical drunk driving behavior related to lane position maintenance, speed control, judgment, and vigilance.[9]

Out of these four technology categories, the Driver Alcohol Detection System for Safety (DADSS) has chosen only tissue-spectrometry-based TruTouch and distant-spectrometry-based Autoliv technologies for prototype development. TruTouch, operating in the NIR range of 1.25–2.5 μm, transmits light into the skin in contact with an optical touchpad and collects and analyzes the diffusely reflected light to determine the subject's BAC.[10] However, TruTouch's selectivity is limited by weak ethanol absorption in NIR and confounding absorptions from other skin tissue components, such as skin pigments, to which NIR tissue spectroscopy is sensitive. The Autoliv system draws cabin air from the car into its optical module through a breathing cup which is subsequently analyzed by a detector to determine the external concentration of ethanol and CO_2. The approach assumes that alveolar CO_2 concentration remains constant. However, in practice, alveolar CO_2 concentration varies from person to person and with the level of physical activity,[11] which complicates the calibration procedure and introduces false readings.

In comparison, WM-DPTR, a non-invasive, non-contacting, and patented[12] mid-infrared thermophotonic technique for measuring low concentrations of solutes in strongly absorbing fluids like water and blood, presents itself as a very promising technology for alcohol detection and can

a)mandelis@mie.utoronto.ca

 © 2015 AIP Publishing LLC

overcome the abovementioned difficulties. Its unique photothermal signal generation properties enable it to overcome the shallow MIR optical penetration depth due to high water absorption and allow for signal amplification due to combined optical and thermal changes of the ISF with BAC. Our previous work[13] has demonstrated the potential and feasibility of the WM-DPTR method for ethyl alcohol detection. In this paper, a calibration method is developed for the WM-DTPR-based alcohol biosensor using a combined theoretical and experimental approach with ethanol and human serum solutions diffused from skin to convert the device into an accurate and precise alcohol detector.

II. METHODS

A. WM-DPTR experimental setup

The WM-DPTR system[12] consists of two quantum cascade lasers (QCL) emitting at the peak (9.5 μm or 1042 cm^{-1}) and at the baseline (10.4 μm or 962 cm^{-1}) of the ethanol mid-infrared absorption band, Fig. 1. The experimental system was shown in Fig. 3 of our previous paper.[13] Two function generators produce a phase-locked square wave to modulate the laser beams and control the phase difference, dP between the beams. The laser modulation frequency which controls the probing depth is set at 90 Hz to generate a probe depth of <40 μm in the epidermis layer and below the stratum corneum to achieve ethyl alcohol detection in the ISF. The type of skin sample has been described in detail in Ref. 13. Briefly, the skin sample was human abdomen skin obtained from abdominal plastic surgery ("tummy tuck" procedure). The freshly harvested human skin with the hypodermis layer removed was fixed and dried between filter paper sheets. The "dry" skin (epidermis + dermis) of ~1 mm thickness was cut into a circular shape of ~25 mm diameter and glued onto the cylindrical cell with the stratum corneum layer facing the laser beam. A motorized variable circular mid-IR neutral density (ND) filter (Reynard Corp., CA) is placed in front of laser B to control the intensity ratio $R = I_A/I_B$ of the two lasers. The differential photothermal radiometry (DPTR) infrared (thermal) photon signal generated by the two out-of-phase square-wave-modulated laser beams irradiating the sample is collected by a pair of parabolic mirrors and focused onto a HgCdZnTe detector with high detectivity in the 2-5 μm spectral range. The output from the MCZT detector is then sent to a lock-in amplifier for demodulation and analysis. Using LabView software, the system includes feedback for controlling the power ratio, R, and phase difference, dP, of the two lasers, henceforth referred to as "the system parameters," through rotational adjustment of the neutral density filter and temporal adjustment of the two square-wave modulation waveforms. Experimental results with the WM-DPTR-based ethanol biosensor used for developing the present calibration method were shown in Fig. 7 of our previous paper.[13] For the given system parameter combinations of (0.99, 180.53°) and (0.96, 180.53°) as the ethanol concentration increases from 0 mg/dl to 100 mg/dl, the differential amplitude V_{AB} decreased by about 83% and the differential phase P_{AB} increased by 150°. Thus, WM-DPTR measurements of ethanol concentrations in the 0-100 mg/dl range are well-resolved for both the amplitude and phase.

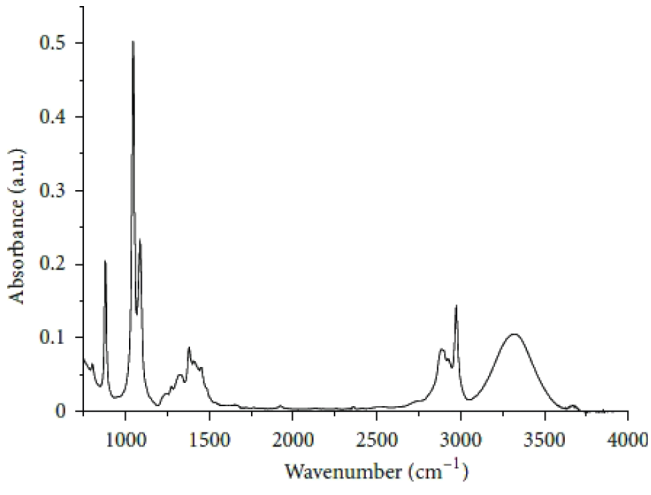

FIG. 1. Mid-infrared optical absorption spectrum of liquid ethanol.[14]

B. WM-DPTR theory

It has been shown[15] that the DPTR signal generated by each laser is given by:

$$\Delta Q_j(t) = \frac{I_o \alpha \mu_{ej} \bar{\mu}_{IR}}{2k} K(\lambda_1\lambda_2)\tau_{tj} \times \left\{ \begin{array}{l} \frac{1}{\bar{\mu}_{IR}+\mu_{ej}}\left[W\left(\sqrt{\frac{t}{\tau_{tj}}}\right)+W\left(\sqrt{\frac{t}{\tau_{IR}}}\right)-2\right] \\ +\frac{1}{\bar{\mu}_{IR}+\mu_{ej}}\left[W\left(\sqrt{\frac{t}{\tau_{tj}}}\right)-W\left(\sqrt{\frac{t}{\tau_{IR}}}\right)\right] \\ +\frac{2}{\bar{\mu}_{IR}}\left\{2\sqrt{\frac{t}{\pi\tau_{tj}}}-\sqrt{\frac{\tau_{IR}}{\tau_{tj}}}\left[1-W\left(\sqrt{\frac{t}{\tau_{IR}}}\right)\right]\right\} \end{array} \right\} \quad (1)$$

with $\Delta QA(t)$ and $\Delta QB(t)$ being the DPTR signal generated by laser A and laser B, respectively; I_o is the laser intensity; α is the thermal diffusivity of the sample; μ_e is its absorption coefficient; $\bar{\mu}_{IR}$ is its spectrally weighted IR emission coefficient; k is its thermal conductivity; $K(\lambda 1, \lambda 2)$ is a factor related to the IR detector bandwidth defined by $[\lambda_1, \lambda_2]$; $\tau_{tj} = (\mu_{ej}^2\alpha)^{-1}$, $j = A, B$, and $\tau_{IR} = (\bar{\mu}_{IR}^2\alpha)^{-1}$ are characteristic photothermal time constants of the absorbing medium; and $W(x) = e^{x^2}\,\mathrm{erfc}(x)$ with $\mathrm{erfc}(x)$ being the complementary error function. In practice, $\bar{\mu}_{IR}$ is a fitting parameter to experimental data.

For the WM-DPTR measurements, only laser A is turned on during $0 \le t \le \tau_p$ while only laser B is turned on during $\tau_p \le t \le \tau_o$ with τ_o being the repetition period of the modulating pulse and $\tau_p = \tau_o/2$. Over the full period $0 \le t \le \tau_o$, the sequence of photothermal responses can be described as:

$$S_{AB}(t) = \begin{cases} \Delta Q_A(t)\,u(t) - \Delta Q_A(t-\tau_p)\,u(t-\tau_p) \\ +\Delta Q_B(t-\tau_p)\,u(t-\tau_p) + \Delta Q_B(t+\tau_p) - \Delta Q_B(t) \end{cases};\quad 0 \le t \le \tau_o \tag{2}$$

where $u(t)$ is the unit step (or Heaviside) function.

In most cases, the transient decays are slow and occur over N periods. Thus, S_{AB} should include contributions from earlier decaying transients from lasers A and B from prior N periods. The complete set of signal contributions from photothermal transients of the earlier periods is:

$$\begin{aligned} S_{AB-0}(t) &= \begin{cases} \Delta Q_A(t)\,u(t) - \Delta Q_A(t-\tau_p)\,u(t-\tau_p) \\ +\Delta Q_B(t-\tau_p)\,u(t-\tau_p) \end{cases};\quad 0 \le t \le \tau_o \\ S_{AB-1}(t) &= \begin{cases} \Delta Q_A(t+\tau_0)\,u(t+\tau_0) - \Delta Q_A(t+\tau_p)\,u(t+\tau_p) \\ +\Delta Q_B(t+\tau_p)\,u(t+\tau_p) - \Delta Q_B(t)\,u(t) \end{cases};\quad -\tau_o \le t \le 0 \\ &\vdots \\ S_{AB-N}(t) &= \begin{cases} \Delta Q_A(t+N\tau_o)\,u(t+N\tau_o) \\ -\Delta Q_A(t+N\tau_o-\tau_p)\,u(t+N\tau_o-\tau_p) \\ +\Delta Q_B(t+N\tau_o-\tau_p)\,u(t+N\tau_o-\tau_p) \\ -\Delta Q_B[t+(N-1)\tau_o]\,u[t+(N-1)\tau_o]\,h_N \end{cases};\quad -N\tau_0 \le t \le -(\mathrm{N}-1)\tau_0 \end{aligned} \tag{3}$$

where

$$h_N = \begin{cases} 1;\ N \ge 1 \\ 0;\ N = 0 \end{cases} \tag{4}$$

and the measured signal is

$$S_{AB}(t) = \sum_{N=0}^{\infty} S_{AB-N}(t). \tag{5}$$

The demodulated signal from the lock-in amplifier is the Fourier transform of the WM-DPTR signal and is expressed as in-phase $\Delta S_{IP}(\omega_o)$ and quadrature $\Delta S_Q(\omega_o)$ channels:

$$\begin{aligned} S_{IP}(\omega_o) &= \frac{2}{\pi} b_1(\omega_o) \\ \Delta S_Q(\omega_o) &= -\frac{2}{\pi} a_1(\omega_o) \end{aligned} \tag{6}$$

with

$$\begin{bmatrix} a_1(\omega_o) \\ b_1(\omega_o) \end{bmatrix} = \frac{\omega_o}{\pi} \int_0^{\tau_o} S_{AB}(t) \begin{bmatrix} \cos(\omega_o t) \\ \sin(\omega_o t) \end{bmatrix} dt \tag{7}$$

which can be recast in terms of amplitude A_{AB} and phase P_{AB}:

$$\begin{aligned} A_{AB} &= \sqrt{\Delta S_{IP}^2 + \Delta S_Q^2} \\ P_{\mathrm{AB}} &= \tan^{-1}\left(\frac{\Delta S_Q}{\Delta S_{IP}}\right). \end{aligned} \tag{8}$$

C. WM-DPTR-based alcohol sensor calibration

A WM-DPTR alcohol biosensor calibrator has been developed through simulation based on the WM-DPTR theory described in the previous section with the differential amplitude and phase calculated using Eq. (8). The IR detector bandwidth factor $\mathrm{K}(\lambda_1,\lambda_2)$ was set to 0.0364 W K^{-1} cm^{-3} and the modulation frequency was set at 90 Hz. The fitting parameter $\bar{\mu}_{IR}$ was varied from 0 to 1000 cm^{-1} to obtain the best fit. This was accomplished by finding the value that gives the minimum mean square error (MMSE) between the calibration curves and ethanol measurement results, optimizing the fitting parameter in the whole range of ~0-100 mg/dl. The optimization could be performed for the ranges of interest by means of the sensitivity tunability property demonstrated in Ref. 13. In the ethanol measurement simulation, the samples, which are solutions with 0-120 mg/dl of ethanol in human blood serum diffused through skin, were excited using two out-of-phase laser beams of wavelengths 9.5 μm and 10.4 μm. The IR detector bandwidth was set to 2-5 μm, consistent with the detection bandwidth of the MCZT detector used in the experimental setup. The lock-in amplifier time constant was set at 10 s and the prior transient period number N was set to 1000.

Appropriate equations were used to model the optical and thermal properties of the sample. The absorption coefficient of the sample was calculated from[16]

$$\mu_e = \sum_i v_i \mu_{e,i} \tag{9}$$

where $\mu_{eA,i}$ is the absorption coefficient and v_i is the volume fraction of the pure component i. The thermal conductivity was computed from[17]

$$k = \sum_i v_i k_i \tag{10}$$

where k_i is the thermal conductivity of the pure component i. The thermal diffusivity was determined from[18]

$$\alpha = \frac{k}{\rho c} = \frac{k}{\sum_i v_i \rho_i c_i} \tag{11}$$

where ρc is the product of density and specific heat capacity of the sample, ρ_i is the density and c_i is the specific heat capacity of the pure component i. The components in the model consist of ethanol, blood serum, and skin. 70.2% is used as the volume fraction of water in the dermis in the simulations.[19]

Values for the thermal and optical properties of ethanol, water, serum, and skin used in the simulator were drawn from various sources. The ethanol absorption coefficient was

TABLE I. Optical and thermal properties with varying ethanol concentration in human serum solutions diffused through skin.

CETOH (mg/dl)	μ_{eA} (cm^{-1})	k (10^{-3} W/cm K)	α (10^{-3} cm^2/s)
0	832.1	5.230	1.3231
20	832.0	5.229	1.3230
40	831.9	5.228	1.3229
60	831.8	5.227	1.3229
80	831.7	5.227	1.3228
100	831.6	5.226	1.3228
120	831.5	5.225	1.3227

obtained from the NIST Chemistry WebBook,[20] the water spectrum from Wieliczka *et al.*,[21] the thermal properties of ethanol-water from measurements by Wang and Fiebig,[22] the thermal properties of skin from Dai *et al.*,[23] the optical properties of skin from Michel *et al.*,[24] the thermal properties of human serum from data on IT'IS Foundation database,[25] and the optical properties of human serum from the work by Giovenale *et al.*[26] The optical and thermal properties of human serum with different concentrations of ethanol CETOH diffused from skin are listed in Table I. From our previous FTIR measurements (Fig. 2 of Ref. 13) it can be seen that the absorption curves barely change at 10.4 μm when ethanol concentration increases from 0% to 50%. Thus we assume the absorption coefficient μ_{eB} does not change when ethanol concentration changes from 0 to 100 mg/dl. Quantitatively speaking, from Refs. 20 and 21, $\mu_{water\ B} \approx 735.5\ cm^{-1}$ while $\mu_{pure\ ethanol\ B} \approx 4.7\ cm^{-1}$. Since, in our calibrations, the highest ethanol concentration is 120 mg/dl, the largest change in μ_{eB} due to change in ethanol concentration is less than 0.6 cm^{-1}, which is very small compared to $\mu_{water\ B}$. Thus, taking μ_{eB} as constant for all ethanol concentrations has no or almost no impact on the fitting results.

D. Ethanol concentration estimation

The developed ethanol concentration estimator uses the ethanol calibration curves to estimate BAC based on both the measured amplitude and phase. It takes the weighted average of BAC estimated using the measured amplitude, $BAC_{amplitude}$, and phase, BAC_{phase}, to obtain an estimated ethanol concentration. Importantly, it takes advantage of the WM-DPTR amplitude and phase complementary sensitivity to optimize the accuracy and precision of the developed biosensor. The amplitude of the differential signal has higher sensitivity at low ethanol concentrations while the phase exhibits higher sensitivity at high concentrations. Therefore, more weight is assigned to $BAC_{amplitude}$ if the estimated BAC is in the low ethanol concentration range and more weight to BAC_{phase} in the high ethanol concentration range. A threshold value is used to determine these low and high ethanol concentration ranges. Setting the threshold value to 50 BAC gave the best results. The estimated BAC is calculated as follows.

$$Estimated\ BAC = \beta BAC_{amplitude} + (1-\beta)\, BAC_{phase}. \quad (12)$$

TABLE II. Ethanol concentration estimation using a common fitting parameter value for the amplitude and phase with the system parameter combination of R = 0.99, dP = 179.68°.

Actual ethanol concentration (mg/dl)	Estimated ethanol concentration (mg/dl)	Accuracy (systematic error in mg/dl)	Precision (standard deviation in mg/dl)
0	0.00	0.00	0.00
20	19.36	0.64	0.33
60	59.98	0.02	0.61
100	99.76	0.24	0.06

III. RESULTS AND DISCUSSION

Figure 2 shows the calibration curve with the experimental results when the fitting parameter $\bar{\mu}_{IR}$ is set to 141 cm^{-1} for the best overall fit for both the amplitude and phase. After varying β between 0 and 1, it was found that the smallest mean absolute error and mean variance were obtained when setting β to 0.74 for low ethanol concentrations and 0.06 for high ethanol concentrations. As shown in Fig. 2, the calibration curves and experimental ethanol measurement results have similar overall shapes. Both the amplitude and the phase of the differential signal decrease monotonically with increasing ethanol concentration. Table II shows the alcohol biosensor performance if the calibration curves in Fig. 2 are used for ethanol concentration estimation. The mean absolute error and mean variance (a measure of biosensor precision) between

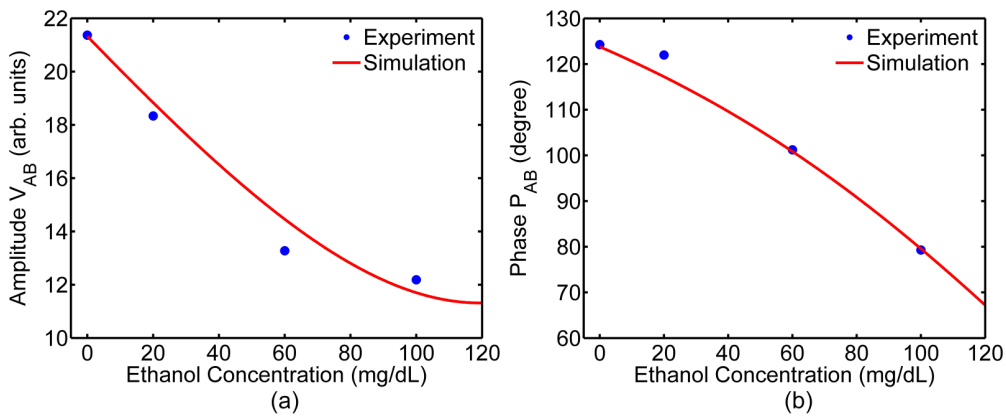

FIG. 2. Ethanol calibration curves using a common fitting parameter value for the amplitude and phase with the system parameter combination of R = 0.99, dP = 179.68°: (a) amplitude and (b) phase.

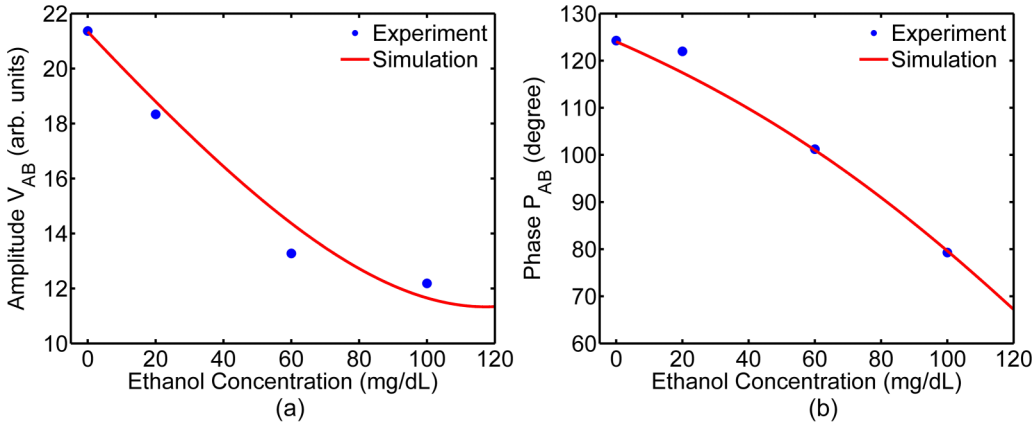

FIG. 3. Ethanol calibration curves using different fitting parameter values for the amplitude and phase with the system parameter combination of R = 0.99, dP = 179.68°: (a) amplitude and (b) phase.

TABLE III. Ethanol concentration estimation using different fitting parameter values for the amplitude and phase with the system parameter combination of R = 0.99, dP = 179.68°.

Actual ethanol concentration (mg/dl)	Estimated ethanol concentration (mg/dl)	Accuracy (systematic error in mg/dl)	Precision (standard deviation in mg/dl)
0	0.00	0.00	0.00
20	19.50	0.50	0.28
60	60.11	0.11	0.63
100	100.13	0.13	0.02

estimated BAC using Eq. (12) and experimental data from Fig. 2 are 0.23 mg/dl and 0.12 mg/dl, respectively, with the above fitting parameter $\bar{\mu}_{IR}$ and β settings.

To improve the results, the fitting parameters were optimized separately for the amplitude and phase. Fig. 3 shows the calibration results when the amplitude fitting parameter $\bar{\mu}_{IR}$ is set at 174 cm^{-1} for the best amplitude fit and the phase fitting parameter $\bar{\mu}_{IR}$ is set at 129 cm^{-1} for the best phase fit. In addition, β is set at 0.75 for low ethanol concentrations and at 0.04 for high ethanol concentrations for the lowest mean absolute error and mean variance. The ethanol concentration estimation results are shown in Table III. The mean absolute error and mean variance between estimated BAC using Eq. (12) and experimental data from Fig. 3 are

TABLE IV. Comparison with other alcohol biosensors—systematic error.[a]

		Autoliv[9]	TruTouch[9]	WM-DPTR	DADSS specifications[9]
Ethanol concentration	0			0.00	1
	20	0.2		0.50	1
	60			0.11	0.7
	80	0.8	0.1		0.3
	100			0.13	
	120	0.0			1
In vivo or *in vitro*		*In vitro*	*In vitro*	*In vitro*	
Measurement time		5 s	30 s	120 s	325 ms

[a]Unit for systematic error: mg/dl. Shaded areas: Information is not available.

TABLE V. Comparison with other alcohol biosensors—standard deviation.[a]

		Autoliv[9]	TruTouch[9]	WM-DPTR	DADSS specifications[9]
Ethanol concentration	0			0.00	1
	20	1.7		0.28	1
	60			0.63	0.7
	80	2.2	1.6		0.3
	100			0.02	
	120	2.7			0.1
In vivo or *in vitro*		*In vitro*	*In vitro*	*In vitro*	
Measurement time (s)		5	5	30	120

[a]Unit for standard deviation: mg/dl. Shaded areas: Information is not available.

0.19 mg/dl and 0.12 mg/dl, respectively, when the optimal fitting parameter $\bar{\mu}_{IR}$ and β settings are selected.

Tables IV and V compare the accuracy and precision of the developed alcohol biosensor with those of commercial alcohol biosensors: *in vitro* measurement performance and DADSS specifications. The developed WM-DPTR-based alcohol biosensor exceeds the DADSS specifications in terms of both accuracy and precision for all measured ethanol concentrations. Its accuracy is comparable to other technologies, but its precision can outperform all other technologies for all measured ethanol concentrations. In terms of measurement time, the commercial biosensors can determine ethanol concentration in a time frame on the order of seconds. For ethanol measurements using the WM-DPTR-based biosensor, a large (10 s) lock-in time constant was used to ensure signal stability since aged lasers were used during the measurement leading to a long delay in lock-in amplifier steady measurements and resulting in a measurement time of about 2 min. This record can be vastly improved with state-of-art QCL technology.

IV. CONCLUSIONS

A calibration method based on WM-DPTR theory and on experimental data has been introduced to convert WM-DPTR measurements into a quantitative ethyl alcohol biosensor. The calibrated biosensor exhibits very-good-to-excellent alcohol concentration accuracy in the case of ethanol and human serum solutions diffused through skin: it can achieve a high accuracy of 0.19 mg/dl in the mean absolute error which is comparable to state-of-the-art commercial non-invasive ethanol sensors. Furthermore, it outperforms other alcohol detection technologies in terms of precision, achieving a high precision of 0.12 mg/dl in mean variance. If best-fits of the experimental data to WM-DPTR theory are performed separately for the amplitude and phase, they result in better fits between calibration curves and experimental results, thereby improving the performance of the biosensor. It is expected that the ethanol concentration measurement time using the WM-DPTR-based biosensor will decrease substantially with state-of-the-art quantum cascade lasers.

ACKNOWLEDGMENTS

The authors wish to acknowledge the Natural Sciences and Engineering Research Council of Canada (NSERC) for financial support of this research project through Engage and Discovery grants to A.M.

[1]S. Perreault, Impaired driving in Canada, 2011, Statistics Canada—Catalogue No. 85–002-X, 2013.
[2]Impaired Driving in Canada, Drunk Driving in Canada Finding an Impaired Driving Lawyer, 2014, http://www.dui.ca.
[3]C. Willis, S. Lybrand, and N. Bellamy, Cochrane Database Syst. Rev. **18**, CD004168 (2004).
[4]G. A. Beitel, M. C. Sharp, and W. D. Glauz, Inj. Prev. **6**, 158 (2000).
[5]J. O'Donnell, Will All Autos Some Day Have Breathalyzers? 2006, http://usatoday30.usatoday.com/money/autos/2006-04-24-breathalyzer-usat_x.htm.
[6]S. A. Ferguson and E. Traube, Using Technology to Eliminate Drunk Driving, 2010, http://www.nhtsa.gov/DOT/NHTSA/NVS/Public%20Meetings/Presentations/2010%20Meetings/HyundaiDADSS.pdf.
[7]S. A. Ferguson, E. Traube, A. Zaouk, and R. Strassburger, in *Proceedings of the 21st International Technical Conference on the Enhanced Safety of Vehicles*, *Stuttgart, Germany* (NHTSA, 2009), pp. 09–0464.
[8]T. D. Ridder, B. J. Ver Steeg, S. J. Vanslyke, and J. F. Way, Proc. SPIE **7186**, 71860E (2009).
[9]S. A. Ferguson, A. Zaouk, N. Dalal, C. Strohl, E. Traube, and R. Strassburger, in *Proceedings of the 22nd International Technical Conference on the Enhanced Safety of Vehicles*, *Washington, DC, USA* (NHTSA, 2011), pp. 11–0230.
[10]M. Venugopal, K. E. Feuvrel, D. Mongin, S. Bambot, M. Faupel, A. Panangadan, A. Talukder, and R. Pidva, IEEE Sens. J. **8**, 71 (2008).
[11]B. Hök, H. Pettersson, and G. Andersson, in *Proceedings of Microstructure Workshop*, *Västerås, Sweden* (NHTSA, 2006), p. 36-Ble.
[12]A. Mandelis and X. Guo, U.S. patent 08649835 Cl. 600–316 (11 February 2014).
[13]X. Guo, A. Mandelis, Y. Liu, B. Chen, Q. Zhou, and F. Comeau, Biomed. Opt. Express **5**, 2333 (2014).
[14]I. Doroshenko, V. Pogorelov, and V. Sablinskas, Dataset Pap. Chem. **2013**, 329406 (2013).
[15]A. Mandelis and X. Guo, Phys. Rev. E **84**, 041917 (2011).
[16]S. L. Jacques, Phys. Med. Biol. **58**, R37 (2013).
[17]C. Richter, H. J. Viljoen, and N. F. J. V. Rensburg, J. Appl. Phys. **93**, 2663 (2003).
[18]A. Matvienko and A. Mandelis, Int. J. Thermophys. **26**, 837 (2005).
[19]A. N. Bashkatov, E. A. Genina, and V. V. Tuchin, J. Innovative Opt. Health Sci. **4**, 9 (2011).
[20]S. E. Stein, "Infrared spectra," in *NIST Chemistry WebBook, NIST Standard Reference Database Number 69*, edited by P. J. Linstrom and W. G. Mallard (NIST Mass Spectrometry Data Center, National Institute of Standards and Technology, 2003), http://webbook.nist.gov.
[21]D. M. Wieliczka, S. Weng, and M. R. Querry, Appl. Opt. **28**, 1714 (1989).
[22]J. Wang and M. Fiebig, Int. J. Thermophys. **16**, 1353 (1995).
[23]T. Dai, B. M. Pikkula, L. V. Wang, and B. Anvari, Phys. Med. Biol. **49**, 4861 (2004).
[24]A. P. Michel, S. Liakat, K. Bors, and C. F. Gmachl, Biomed. Opt. Express **4**, 520 (2013).
[25]P. A. Hasgall, E. Neufeld, M. Gosselin, A. Klingenbock, and N. Kuster, IT'IS Database for Thermal and Electromagnetic Parameters of Biological Tissues, version 2.6, IT'IS Foundation, 2015, http://www.itis.ethz.ch/database.
[26]E. Giovenale, M. D'Arienzo, A. Doria, G. P. Gallerano, A. Lai, G. Messina, and D. Piccinelli, J. Biol. Phys. **29**, 159 (2003).